Biogeosciences

Open Access

Modeling light use efficiency in a subtropical mangrove forest equipped with CO_2 eddy covariance

J. G. Barr[1], **V. Engel**[2], **J. D. Fuentes**[3], **D. O. Fuller**[4], **and H. Kwon**[5]

[1]South Florida Natural Resource Center, Everglades National Park, Homestead, FL 33030, USA
[2]Southeast Ecological Science Center, US Geological Survey, Gainesville FL 32653, USA
[3]Department of Meteorology, The Pennsylvania State University, University Park, PA 16802, USA
[4]Department of Geography and Regional Studies, University of Miami, Coral Gables, FL 33124, USA
[5]Department of Civil Engineering, Chonbuk National University, Jeonju, South Korea

Correspondence to: J. G. Barr (jordan_barr@nps.gov)

Abstract. Despite the importance of mangrove ecosystems in the global carbon budget, the relationships between environmental drivers and carbon dynamics in these forests remain poorly understood. This limited understanding is partly a result of the challenges associated with in situ flux studies. Tower-based CO_2 eddy covariance (EC) systems are installed in only a few mangrove forests worldwide, and the longest EC record from the Florida Everglades contains less than 9 years of observations. A primary goal of the present study was to develop a methodology to estimate canopy-scale photosynthetic light use efficiency in this forest. These tower-based observations represent a basis for associating CO_2 fluxes with canopy light use properties, and thus provide the means for utilizing satellite-based reflectance data for larger scale investigations. We present a model for mangrove canopy light use efficiency utilizing the enhanced green vegetation index (EVI) derived from the Moderate Resolution Imaging Spectroradiometer (MODIS) that is capable of predicting changes in mangrove forest CO_2 fluxes caused by a hurricane disturbance and changes in regional environmental conditions, including temperature and salinity. Model parameters are solved for in a Bayesian framework. The model structure requires estimates of ecosystem respiration (R_E), and we present the first ever tower-based estimates of mangrove forest R_E derived from nighttime CO_2 fluxes. Our investigation is also the first to show the effects of salinity on mangrove forest CO_2 uptake, which declines 5 % per each 10 parts per thousand (ppt) increase in salinity. Light use efficiency in this forest declines with increasing daily photosynthetic active radiation, which is an important departure from the assumption of constant light use efficiency typically applied in satellite-driven models. The model developed here provides a framework for estimating CO_2 uptake by these forests from reflectance data and information about environmental conditions.

1 Introduction

Mangrove forests have received significant attention recently due to an increased recognition of the role these systems play in global carbon (C) cycles (Donato et al., 2011). However, compared to terrestrial systems, the processes that regulate ecosystem–atmosphere carbon dioxide (CO_2) fluxes, including gross primary productivity (GPP) and ecosystem respiration (R_E), are not well understood. Tower-based, eddy covariance (EC) measures of the net (i.e., GPP–R_E) ecosystem–atmosphere CO_2 exchange (or NEE) in conjunction with continuous measurements of environmental variables were started only recently compared to terrestrial systems (see Barr et al., 2010) and remain extremely rare. These observations show that canopy-scale CO_2 fluxes are influenced by stressors that are unique to mangrove forests, including periodic flooding and variable soil pore water salinity. Using these EC data to calculate canopy-level light use efficiency (LUE, defined as GPP divided by incoming photosynthetic active radiation (PAR)) will improve our understanding of C cycling in these forests. Modeling canopy-level LUE in

relation to PAR and ground-based scalars in turn provides a first step towards using satellite reflectance data to define the larger role these forests play in both regional and global C budgets. However, typical LUE models developed for terrestrial systems do not account for the unique factors that influence C dynamics in tidal forests, and new approaches are needed.

For all plant communities, including mangrove forests, the net ecosystem carbon balance (NECB, or the C accumulating in plants and soils; Chapin et al., 2006) can be estimated using the following expression:

$$NECB = -NEE + F_{DIC} + F_{DOC} + F_{POC} + F_{CO} + F_{CH_4} + F_{VOC} \quad (1)$$

where all terms in Eq. (1) are expressed in $g\,C\,m^{-2}\,t^{-1}$. The F_{DIC}, F_{DOC}, and F_{POC} are the net lateral exchanges of dissolved inorganic C (DIC), organic C (DOC), and particulate organic C (POC). The F_{CO}, F_{CH_4}, and F_{VOC} are net absorption (or efflux (negative sign)) of carbon monoxide (CO), methane (CH_4), and volatile organic C (VOC), respectively. Methanogenesis is generally considered negligible for mangrove soils, where sulfate reduction prevents bacterial production of CH_4 (Strangmann et al., 2008). Mangrove foliage emits several biogenic hydrocarbons (Barr et al., 2003), but fluxes were several orders of magnitude smaller than leaf-level CO_2 carboxylation rates. Carbon monoxide was produced from the photodegradation of chromophoric dissolved organic matter (CDOM) derived from red mangrove leaf litter (Shank et al., 2010). While it is generally recognized that mangrove forests are sources of CO, CH_4, and VOC, their contribution to the carbon budget (Eq. 1) has not been quantified. Negative NEE values represent a loss of C as CO_2 from the atmosphere, and negative F values represent C loss from the ecosystem. In terrestrial systems with minimal F, positive nighttime NEE values are considered a proxy for R_E. Compared to terrestrial systems, mangrove forests are characterized by low nighttime NEE, large daytime –NEE values and large $-F$ (Barr et al., 2012). However, comprehensive in situ measures of mangrove forest C dynamics that simultaneously account for both vertical C fluxes (i.e., NEE) and lateral C fluxes (F) have not been attempted. Continuous and long-term estimates of F_{DIC}, F_{DOC}, and F_{POC} usually do not exist. Instead, lateral C fluxes are ordinarily determined only during short-term intensive field campaigns (e.g., Romigh et al., 2006; Alongi et al., 2004; Souza et al., 2009; Mayorga et al., 2005). In the absence of these measurements, nighttime, tower-based NEE estimates in many mangrove forests cannot be used as a direct proxy for R_E as they are in terrestrial systems, since the actual ecosystem-scale respiratory CO_2 fluxes in tidal systems will also include respiratory fluxes derived from F transported outside of the EC footprint. Nonstandard methods for calculating R_E, and therefore GPP, are required in mangrove forests utilizing EC.

Monteith (1966, 1972) first proposed the concept of relating GPP to PAR through a light use efficiency term, ε, or multiplicative efficiency terms. Light use efficiencies describe the process of light absorption by green vegetation and photosynthetic CO_2 assimilation by foliage. Light use efficiency terms in ecosystem models (e.g., Xiao et al., 2004; Cook et al., 2008; Potter, 2010) are calculated in a two-step process. First, functional relationships are established between environmental drivers, such as temperature and water stress, that regulate physiological functioning and thus GPP. A second step is to determine how much of the incident solar irradiance is absorbed by photosynthetic active green vegetation. Useful proxies for the process of light absorption by vegetation can be determined using remote sensing information (Zhao and Running, 2008). In one of the first attempts to incorporate remote sensing information into ecosystem models, Tucker et al. (1983) estimated the productivity of grasslands using the normalized difference vegetation index (NDVI) from the Advanced Very High Resolution Radiometer (AVHRR) aboard polar-orbiting platforms. Several other models have been tested and validated using relationships between remote sensing information and ground-based C flux data (Heinsch et al., 2006; Turner et al., 2006; Zhao et al., 2005). More recently, Chen et al. (2010) applied the enhanced vegetation index (EVI) as input into a vegetation photosynthesis model (VPM, Xiao et al., 2004) to take advantage of the high return frequency (1–2 per day) of the Moderate Resolution Imaging Spectroradiometer (MODIS) and the increased spatial resolution (30 m) of LANDSAT. However, the usefulness of satellite reflectance-driven models such as these developed for simulating terrestrial GPP, such as the MODIS GPP product (http://modis.gsfc.nasa.gov/data/dataprod/nontech/MOD17.php) has not been determined for mangrove forests. These types of models are needed to better integrate estimates of mangrove forest CO_2 assimilation patterns across tropical and subtropical coastal zones into global-scale C balance calculations. Therefore, the objectives of this study are the following: (1) to calculate R_E and GPP in a tidal mangrove forest using a novel application of EC-based estimates of NEE, (2) to parameterize and test a model of daily canopy GPP and LUE driven by satellite reflectance data, and (3) to compare these GPP estimates to the MODIS GPP product for this location.

2 Methods

2.1 Site description and meteorological and eddy covariance measurements

The study site (25.3646° N, 81.0779° W), located within Everglades National Park, is near the mouth of the Shark River and ∼ 4 km from the Gulf of Mexico (Fig. 1). The on-site 30 m eddy covariance tower is colocated with long-term monitoring sites operated by the Florida Coastal Everglades Long Term Ecological Research (FCE LTER, site SRS6) program and the US Geological Survey (site SH3). Around the tower site, the dominant mangrove species include
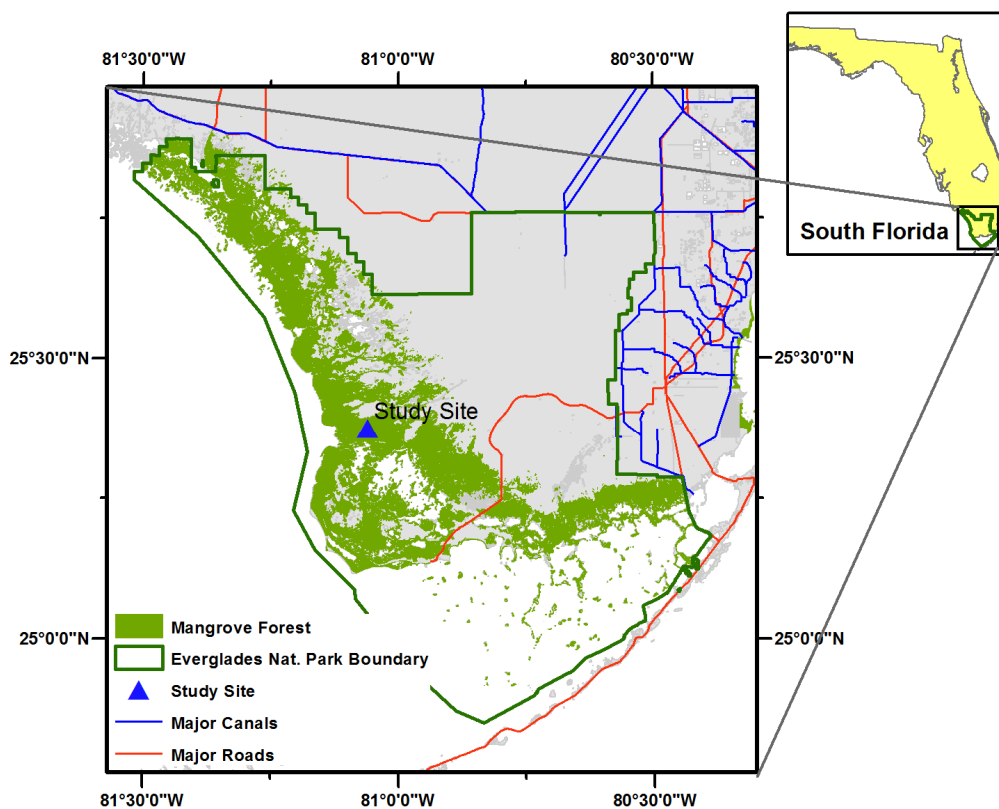
Fig. 1. Map of Everglades National Park, showing mangrove forest zones along the coast, the study site, and the park boundaries, defined by the thick green line. The 30 m EC tower, SRS6, and SH3 are colocated at the study site.

Rhizophora mangle, *Avicennia germinans*, and *Laguncularia racemosa*, and their maximum heights reach about 19 m. Meteorological measurements and EC observations to determine NEE have been made since 2003 at a height of 27 m.

During October 2005 the forest experienced a major disturbance caused by Hurricane Wilma. The disturbance caused major defoliation of the forest and tree mortality, with 25 % of stems > 1.5 m in height being destroyed by the hurricane winds (Barr et al., 2012). Following Hurricane Wilma, instruments were deployed on a new 30 m tower with renewed measurements beginning in November 2006 (Barr et al., 2012). Continuous meteorological measurements are recorded as 1 min averages on data loggers (model CR3000, Campbell Scientific, Inc., Logan, UT), and stored in files saved at 30 min intervals in a laptop computer located on site. High-frequency (10 Hertz) EC data are stored directly on the laptop computer for subsequent processing to derive 30 min average fluxes (using Matlab code, The Mathworks, Inc., Natick, MA), following the protocols employed by scientists associated with the AmeriFlux network (http://public. ornl.gov/ameriflux/index.html). Data gap-filling procedures were implemented to produce continuous time series. Addi-

tional details for site characteristics and data processing protocols are provided in Barr et al. (2010, 2012).

2.2 Partitioning NEE into R_E and GPP

Estimates of ecosystem respiration (R_E; $\mu mol\,CO_2\,m^{-2}\,s^{-1}$) are needed to calculate GPP ($\mu mol\,CO_2\,m^{-2}\,s^{-1}$), which is defined as GPP $= -NEE + R_E$. In tidal mangrove forests equipped with EC, nighttime NEE can be considered as a proxy for nighttime R_E only when the sediment surface is exposed to the atmosphere during low tides. NEE represents the EC-derived CO_2 flux at a height of 27 m plus the amount of CO_2 stored in a column of air below this height since the previous time step. This storage was estimated from the change in CO_2 mixing ratio at the infrared gas analyzer level of 27 m (Barr et al., 2010). When the sediment surface is inundated during a flood tide, a fraction of the CO_2 respired by soil, roots, and detritus is dissolved in the overlying water column and transported into the adjacent estuary as DIC during the subsequent ebb tide. Therefore, tower-based nighttime NEE $\neq R_E$ when the surface is inundated. To correct for this effect in our calculations of GPP, nonlinear least-squares regression analyses were performed to express nighttime R_E as a function of air temperature, T_A (after Reichstein et al., 2005), using only valid NEE values determined

when the sediment surface was exposed (Fig. 2). Regression analyses of nighttime NEE as a function of T_A during high tides show significantly different relationships than at low tide and are included in Fig. 2 for comparison. High-tide data were excluded from our calculations and the function relating low-tide R_E to T_A was used to gap-fill these periods. Data gaps occurring when the EC system was not operating, or when there was insufficient turbulence ($u^* < 0.14\,\mathrm{m\,s^{-1}}$; Barr et al., 2012) and when the flux footprint included large contributions from adjacent rivers (Barr et al., 2010), were also filled using this function. The R_E function in Eq. (2) includes both an Arrhenius-type activation component and a high-temperature deactivation response.

$$R_E = R_{E20} \exp\left(E_0 \left(\frac{1}{T_{REF} - T_0} - \frac{1}{T_A - T_0} \right) \right) \Big/ \tag{2}$$
$$(1 + \exp\left(E_D (T_A - T_D) \right))$$

The R_{E20} ($\mu\mathrm{mol\,(CO_2)\,m^{-2}\,s^{-1}}$) represents the ecosystem-level respiration rate at the reference air temperature, T_{REF}, which is set as 293.15 K. This R_{E20} value differs from the more common reference temperature of 283.15 K (Lloyd and Taylor, 1994) because it is a closer approximation of the minimum temperature range frequently observed in this forest. Also, the R_E was related to air temperature rather than the more prevalently used soil temperature (Lloyd and Taylor, 1994). The use of air rather than soil temperature was justified by considering the sources contributing to R_E. Foliage respiration alone can contribute 73 % of the total R_E during low-tide periods at night (Barr et al., 2010). Measurements of soil respiration in relatively undisturbed mangrove forests throughout the Caribbean, Australia, and New Zealand (Lovelock, 2008) suggest that soils contribute less respired CO_2 to R_E compared to that of aboveground sources. However, the fractional contribution of the soil to R_E may increase as a result of hurricanes or other disturbances. Soil respiration increased by 18 % in a dry tropical forest in Mexico one year following disturbance from Hurricane Wilma (Vargas and Allen, 2008).

In Eq. (2) the E_0 (K) and E_D (K) parameters are temperature-dependent activation energy and deactivation sensitivity, respectively. The T_0 (K) also accounts for changes in activation energy associated with variations in temperature. Its expected values range between 0 K and observed air temperature (Lloyd and Taylor, 1994). The T_D (K) term is the temperature at which deactivation occurs, and represents a unique feature in this study that explicitly accounts for a reduction in respiration above a threshold temperature. The deactivation term, represented by the denominator in Eq. (2), is assumed equivalent to the relationship describing foliage carboxylation and dark respiration rates (Campbell and Norman, 1998). The response of R_E to temperature is a dynamic process, and consequently the fitted characteristics in Eq. (2) are expected to change seasonally. To capture such variability in respiratory responses, values of R_E and regression characteristics (e.g., R_{E20}, E_0, T_0, E_D, T_D) were determined for a 3-day moving window using nighttime data during low-tide periods from a 15 day centered window. Similar to the findings of Reichstein et al. (2005), a window size of 15 days was sufficiently long to provide adequate data and temperature range for performing the nonlinear regression of Eq. (2) and short enough to minimize the confounding seasonal changes in respiration response. During each 3-day period, the relationship in Eq. (2) was used to compute half-hourly daytime R_E, and half-hourly GPP values were computed as the difference between R_E and daytime NEE (i.e., GPP $= -$NEE $+ R_E$). Half-hourly values of GPP ($\mu\mathrm{mol\,C\,m^{-2}\,s^{-1}}$) were summed as shown in Eq. (3) to provide daily GPP and 8-day average values in units of $\mathrm{mol\,C\,m^{-2}}$ per day. This 8-day time step matches that of the MODIS product and removes noise in the daily data, while retaining seasonal trends. The coefficient of 0.0216 in Eq. (3) converts units of $\mu\mathrm{mol\,CO_2\,m^{-2}\,s^{-1}}$ to $\mathrm{g\,C\,m^{-2}}$ per each 30 min flux averaging interval.

$$GPP = 0.0216 \sum_{i=1}^{48} GPP_{30\,min} \tag{3}$$

2.3 Albedo, EVI, and MODIS GPP

We investigate seasonal changes in canopy structural properties using two measures of canopy reflectance: albedo and EVI. The surface albedo (Fig. 3a) was estimated as the ratio of reflected to incoming solar irradiance measured above the canopy. The adjusted albedo was estimated as the average of albedo values for the periods when the solar elevation angle ranged between 35 and 50°. This adjustment was necessary to remove the influence of changing daily solar elevation angles over the course of the study.

The MODIS EVI product was used to examine seasonal patterns in the mangrove canopy reflectance properties. It is well established (Huete et al., 2002; Jiang et al., 2008) that the EVI data are more reliable compared to NDVI in environments with high biomass content. For this study the EVI data (Fig. 3b) were obtained from the MOD13A1 product (EOS; http://modis.gsfc.nasa.gov/). The mangrove flux tower site is included in grid h10v06, with a 500 m spatial resolution. Using GIS (geographic information system) software (Matlab Mapping Toolbox, The Mathworks, Inc., Natick, MA), the 16-day composite average EVI values for the pixel corresponding to the flux tower site and the 8 adjacent pixels were extracted for the period 2000 to 2011. This 9-pixel domain approximates the extent of the EC measurement footprint (see Fig. 1 in Barr et al., 2010). The MODIS GPP product, MOD17A2 (https://lpdaac.usgs.gov), was also extracted from grid h10v06 for comparison with estimated and modeled GPP in this study. MODIS GPP represents a 16-day composite average with a 1 km spatial resolution. Values were averaged for the pixel corresponding to flux tower site and 4 adjacent pixels included within the measurement footprint and not centered over water.

2.4 LUE modeling framework

The mangrove vegetation photosynthesis light use efficiency model (MVP-LUE) presented here is based on the production efficiency modeling (PEM) framework (Prince and Goward, 1995; Running et al., 1999, 2000). It has the basic form of

$$\text{LUE} = \sum \text{GPP} / \sum \text{PAR} = \varepsilon_g \times \text{fPAR}, \tag{4}$$

where LUE $(\text{mol C} \, (\text{mol photons})^{-1})$ is calculated as the ratio of 8-day sums of GPP to PAR $(\text{mol (photons)} \, \text{m}^{-2})$. The ε_g is a quantum efficiency $(\text{mol C} \, (\text{mol photons})^{-1})$ that describes conversion of absorbed PAR into gross primary production specific to the irradiance incident on green vegetation. fPAR (unitless) is the ratio (8-day average) of PAR absorbed by green vegetation to total incident PAR determined above the vegetated landscape. Previous modeling studies suggested that fPAR linearly increased with EVI (Xiao et al., 2004) or NDVI (Goetz et al., 1999; Schubert et al., 2010). However, in the present study, fPAR increases in response to increasing EVI as determined from the 500 m spatial resolution data according to

$$\text{fPAR} = 1 - e^{-m_{\text{EVI}} \times \text{EVI}}, \tag{5}$$

where m_{EVI} determines the initial slope of fPAR response to increasing EVI. The rate of increase in 8-day average fPAR to increasing EVI diminishes and is dependent on the value of m_{EVI}. We found that the observed quantum LUE of the mangrove ecosystem approaches some optimum efficiency, ε_0 (defined as the light conditions when maximum NEE is attained). The ε_0 is not known a priori and must be determined from an optimization procedure. Most of the time, environmental conditions are less than optimal, and therefore ε_g is often less than ε_0. The ε_g represents a multiplicative chain of efficiencies (Monteith, 1972) where each f term in the chain accounts for a reduction in quantum LUE below ε_0.

Several variables contribute to reducing the quantum efficiency in this forest. The first is elevated foliage temperature resulting from air temperatures $(T_A > 303 \, \text{K})$ which elicit suboptimal carboxylation rates (Barr et al., 2010). Such responses to elevated temperature can be expressed by the relationship shown in Eq. (6) formulated by Raich et al. (1991):

$$f_{T_A} = \frac{(T_A - T_{\text{Min}}) (T_A - T_{\text{Max}})}{[(T_A - T_{\text{Min}}) (T_A - T_{\text{Max}})] - (T_A - T_{\text{Opt}})^2}, \tag{6}$$

where T_A is air temperature recorded at 27 m above the ground (Fig. 4a), and T_{Min}, T_{Max}, and T_{Opt} are minimum, maximum, and optimal temperatures for GPP, respectively. The function f_{T_A} attains the value of 1 when T_A becomes the same as T_{Opt} and is set to zero for $T_A < T_{\text{Min}}$. Raich et al. (1991) determined GPP as a function of temperature for several vegetation types in South America, including tropical evergreen forests, grasslands, and temperate forests.

To compare the temperature dependency of productivity that occurred independently of the magnitude of GPP, ratios of GPP to site-specific maximum GPP $(\text{GPP}_{\text{Max}})$ were compared. All three vegetation types exhibited ratios (i.e., $\text{GPP} / \text{GPP}_{\text{Max}}$) that followed the relationship in Eq. (6), but each possessed its own unique characteristics $(T_{\text{Min}}, T_{\text{Max}},$ and $T_{\text{Opt}})$. While this relationship in Eq. (6) was not previously quantified for the mangrove ecosystem, the shape of the curve is consistent with –NEE response to T_A during 2004–2005 (see Fig. 6 in Barr et al., 2010) for conditions when PAR $> 1000 \, \mu\text{mol (photons)} \, \text{m}^{-2} \, \text{s}^{-1}$.

Barr et al. (2010) showed a linear decline in the 8-day averages of $\text{LUE} / \text{LUE}_{\text{salinity} = 0}$ versus 8-day average soil pore salinity between 10–40 parts per thousand (ppt) of dissolved solutes during both pre- (2004–2005) and post-hurricane (November 2006 to December 2011) periods. This reduction in LUE attributed to changes in salinity (f_{sal}) is defined in Eq. (7). $\text{LUE}_{\text{salinity} = 0}$ was determined from the intercept of the regression.

$$f_{\text{sal}} = 1 - m_{\text{sal}} \times \text{salinity} \tag{7}$$

The m_{sal} defines the rate of decrease in f_{sal} in response to increasing salinity. The decline in LUE with increasing salinity may be partially attributed to photosynthetic saturation under high PAR $(> 50 \, \text{mol photons} \, \text{m}^{-2} \, \text{day}^{-1})$, which coincides with maximal salinity during May and June. A linear function in Eq. (8) was included to account for photosynthesis saturation manifested as declining LUE with increasing PAR.

$$f_{\text{PAR}} = 1 - m_{\text{PAR}} \times \text{PAR} \tag{8}$$

The m_{PAR} defines the rate of decrease in f_{PAR} in response to increasing PAR.

Since fPAR, f_{T_A}, f_{sal}, and f_{PAR} have a maximum value of 1, light use efficiencies approach ε_0 as EVI attains the value of 1, air temperature approaches T_{Opt}, and salinity (ppt) and PAR $(\text{mol photons} \, \text{m}^{-2} \, \text{day}^{-1})$ decrease to zero. The overall resulting quantum efficiency may then be expressed as the multiplicative set of efficiencies to account for the effects of temperature, salinity, and PAR as shown in Eq. (9).

$$\varepsilon_g = \varepsilon_0 \times f_{T_A} \times f_{\text{sal}} \times f_{\text{PAR}} \tag{9}$$

To implement the model described in Eqs. (4) to (9), the individual forcing terms (i.e., ε_0, m_{EVI}, T_{Min}, T_{Max}, T_{Opt}, m_{sal}, m_{PAR}) must be derived from the data through the use of an optimization approach. We apply a Bayesian framework to solve for the posterior probability of model parameters and LUE during the periods 2004–2005 and November 2006 to 2011 when EC-derived estimates of GPP and LUE are available. The Bayesian analytical framework provides several advantages over more traditional model optimization approaches, including the ability to directly estimate uncertainties in modeled LUE without the use of ad hoc procedures. Outputs from the optimization procedure provide the

forcing terms (e.g., m_{EVI}, T_{Opt}, etc.) that are described probabilistically, thereby allowing us to assess the applicability of each term. To cast this model within the Bayesian framework, LUE was considered to exhibit a normal distribution as

$$LUE \sim N(\mu_{LUE}, \sigma_{LUE}), \tag{10}$$

where μ_{LUE} is the time-varying mean and is equal to the expected 8-day average LUE with variance σ_{LUE}. A quantile–quantile (QQ) plot of LUE data against the standard normal distribution was used to verify the normality assumption. The forcing terms were considered to have a prior probability distribution which, when taken together, follow a multivariate normal distribution. That is,

$$\begin{pmatrix} \varepsilon_0 \\ m_{EVI} \\ T_{min} \\ T_{max} \\ T_{opt} \\ m_{sal} \\ m_{PAR} \end{pmatrix} \sim N \begin{pmatrix} \mu_{\varepsilon_0} \\ \mu_{m_{EVI}} \\ \mu_{T_{min}} \\ \mu_{T_{max}} \\ \mu_{T_{opt}} \\ \mu_{m_{sal}} \\ \mu_{m_{PAR}} \end{pmatrix}, \sum \end{pmatrix}, \tag{11}$$

with mean values, μ, and covariance matrix, Σ. Off-diagonal terms in Σ explicitly quantify the interdependence of model forcing terms, if such relationships exist. The inverse Wishart distribution (O'Hagan and Forster, 2004) was used to describe the prior probability distribution of Σ because it represents the conjugate probability distribution of the multivariate normal distribution (Gelman et al., 2004), and expresses the uncertainty about Σ before the data are taken into account. The inverse Wishart distribution represents the multivariate generalization of the scaled inverse-chi-squared distribution, which is the conjugate prior of the univariate normal distribution with unknown mean and variance. The inverse Wishart distribution is defined by its own set of parameters, Ω and ν, commonly referred to as hyperparameters that represent the inverse-scale matrix and degrees of freedom of the distribution, respectively.

$$\Sigma \sim \text{Inv-Wishart}(\Omega, \nu) \tag{12}$$

The Ω was initialized with a 6×6 identity matrix, and the degrees of freedom, $\nu = 6$, representing the number of forcing terms. To learn the optimal probability distributions of the forcing terms (ε_0, m_{EVI}, T_{Min}, T_{Max}, T_{Opt}, m_{sal}), a Markov chain Monte Carlo (MCMC) procedure with Gibbs sampling (Cassella and George, 1992; Gilks et al., 1995) was performed in Matbugs. Matbugs is a Matlab (The Mathworks Inc., Natick, MA) interface to WinBUGS (Spiegelhalter et al., 2003). Gibbs sampling is the simplest of the Markov chain simulation algorithms (Gelman et al., 2004) and is used to directly sample from each conditional posterior distribution in a model. The resulting distribution of the forcing terms maximizes the likelihood that the LUE during the

study period would be observed given the modeled LUE values. The Gibbs sampling procedure within WinBUGS requires initial values (i.e., best guesses) for all the forcing terms. Here, initial values were determined using a constrained optimization technique (Matlab Optimization Toolbox) in minimizing the sum of squared errors (SSE) between modeled and EC estimated 8-day LUE values obtained during the entire study period of 2004–2005 and November 2006 to December 2011. The constrained optimization is useful for obtaining a single point estimate of forcing terms, but does not provide a robust fit that includes the probability distribution of both parameters and modeled LUE values.

3 Results and discussion

3.1 Calculating R_E and GPP from NEE

Temperature, level of inundation, and foliage physiology drive respiration in this forest. Nighttime NEE increased with increasing T_A below $\sim 25\,°C$ during both high- and low-tide periods during 2004–2005 (Fig. 2a). NEE was $\sim 1\,\mu\text{mol}\,(CO_2)\,m^{-2}\,s^{-1}$ higher during low tides, and NEE rates converged at temperatures $> 25\,°C$ for both low- and high-tide periods during 2004–2005 and 2006–2011 (Fig. 2a and b, respectively). The exponential function with deactivation in Eq. (2) generally fit the NEE data during 2004–2005 and 2006–2011 periods (Fig. 2a–d). During 2004–2005, there was some evidence of bimodality in R_E response to temperature with maxima occurring at T_A values ranging between 15 and $20\,°C$ and 25 to $28\,°C$ (Fig. 2a). The NEE was $\sim 1\,\mu\text{mol}\,(CO_2)\,m^{-2}\,s^{-1}$ higher during 2006–2011 compared to 2004–2005 for temperatures above $25\,°C$, possibly due to an increased respiratory contribution from decomposing coarse woody debris (CWD) generated by the hurricane. The hurricane disturbance also resulted in warmer soils during 2006–2011 as more solar irradiance reached the soil surface beneath the damaged canopy (Barr et al., 2012). Such processes contributed to increased nighttime soil–air temperature gradients of 1 to $3\,°C$ one year following disturbance (Table 1, Barr et al., 2012). Warmer soils in this system are expected to lead to increased belowground respiration and fractional increases in the belowground contribution to total nighttime R_E. During both pre- and post-disturbance periods, the functional response of R_E to air temperature exhibited a better fit than that using soil temperature.

The substantial seasonal changes in the respiratory response of the mangrove ecosystem (Fig. 2c, and d) required the use of moving windows to fit Eq. (2) to these data. By partitioning the data by time, particularly into dry and wet season periods, the apparent bimodality of nighttime NEE versus T_A response (Fig. 2a) was no longer apparent in the fitted model. The deactivation term in Eq. (2) that is needed to account for the observed decline in nighttime NEE at elevated T_A represents a unique characteristic of NEE patterns
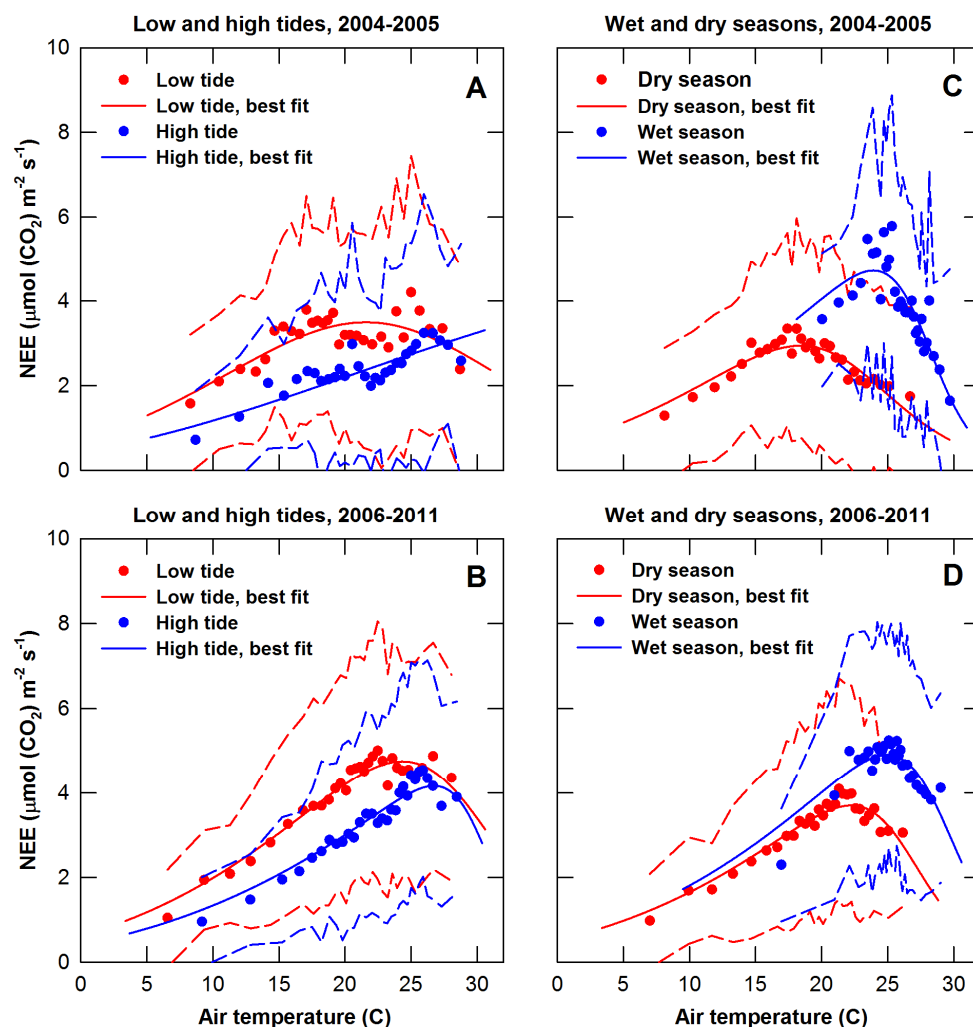
Fig. 2. Nighttime net ecosystem exchange (NEE (μmol (CO$_2$) m^{-2} s^{-1})) versus air temperature at 27 m are partitioned by low- and high-tide periods in 2004–2005 (**A**) and 2006–2011 (**B**), and by dry and wet season months in 2004–2005 (**C**) and 2006–2011 (**D**). Each subset of the data was divided into 30 bins and the average (circles) and ± 1 standard deviation (dashed lines) were computed for each bin. Best-fit lines (Eq. 2) of the half-hourly NEE versus air temperature are included. During low-tide periods, NEE is equivalent to R_E.

at this site compared to terrestrial forests. The temperature that defines the transition from increasing to decreasing respiratory response changed with seasons and as a result of disturbance. The increase in nighttime NEE in response to increasing T_A following the hurricane disturbance was most evident during dry season months, when the values increased by $\sim 1 \, \mu$mol (CO$_2$) m^{-2} s^{-1} as T_A exceeded 20 °C, and continued on an upward trend until reaching a maximum of $\sim 4 \, \mu$mol (CO$_2$) m^{-2} s^{-1} at 22 °C. Before the hurricane disturbance, NEE declined with temperatures exceeding 19 °C. This increase in temperature, which defines peak respiratory response, also suggested an increased contribution of belowground respiration to R_E following disturbance. Quantifying the belowground contribution to R_E and the respiratory response to soil temperature require continuous measurements of belowground respiration, and such measurements were not

made during this study. Due to the long-term nature of this investigation (spanning several years), the ecosystem respiration response captured the broad temperature ranges and levels of inundation experienced by the mangrove forest. As a result, it was possible to identify and quantify the dynamic character of the total respiratory responses, R_E to air temperature and subsequent declines in respiration above T_{opt}.

3.2 Albedo and EVI

Canopy-scale CO$_2$ fluxes in mangrove forests vary seasonally as a result of changes in leaf area index and physiological responses to stressors. Such changes in the amount and function of foliage were inferred from temporal patterns in locally measured surface albedo and the satellite-based greenness index, EVI. Albedo (Fig. 3a) varied seasonally with minimum
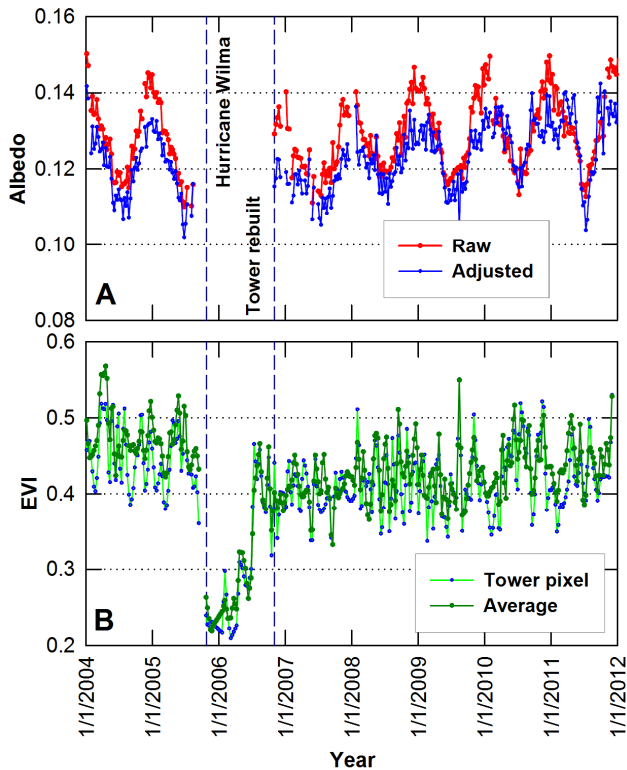
Fig. 3. Eight-day average albedo (raw) and albedo adjusted to include only those values when the solar elevation angle was between 35° and 50° (**A**). Eight-day 500 m resolution EVI (**B**) values were linearly interpolated using 16-day composites. Averages include the pixel that contains the tower site and the adjacent 8 pixels.

values of 0.10 to 0.11 during May and June, and maximum values of 0.13 to 0.15 during December to January. Albedo was about 0.12 during January 2007 and represented a decline of > 0.01 compared to values observed before Hurricane Wilma. Raw and adjusted albedo variability resulted in response to the recovery of foliage from the 2005 disturbance, with apparent full recovery observed by 2011. Structural damage and defoliation of the mangrove forest was evident in the 16-day EVI time series (Fig. 3b) in the days following hurricane disturbance on 24 October 2005. The EVI declined from 0.4–0.5 to 0.22 following the 2005 disturbance. When tower measurements resumed in November 2006, refoliation of surviving branches in the upper canopy and new shoots in the understory had already occurred, with rapid regrowth occurring during June to October 2006. Yet, recovery was incomplete. EVI exhibited a decline of ∼ 12 % when 2007–2008 values were compared with those obtained in 2004–2005. These patterns were consistent with the 30 % lower annual −NEE obtained for 2007. Though noisy, EVI exhibited similar sinusoidal seasonal patterns with maxima and minima values coinciding with the winter and summer solstices, respectively. EVI values represent a much larger area than do the albedo measurements (∼ 250 000 m² (per

pixel), versus ∼ 3000 m², respectively). Such seasonal patterns were consistent with coherent patterns in monthly litter fall rates (Castaneda, 2010) within the flux footprint of the tower site.

3.3 Physical drivers of mangrove productivity

In South Florida, mangroves receive highly variable amounts of PAR (Fig. 4a) resulting from sinusoidal seasonal patterns and cloud cover from localized convective storms during the May to October wet season. The seasonal peak in PAR, and therefore the amount of energy available to drive photosynthesis and GPP, occurred during April and May before the onset of the wet season in late May and June. Air temperatures (Fig. 4b) during March to May were between 25 and 30 °C, and these conditions favored near-optimal foliage carboxylation rates and GPP. However, surface water salinities (Fig. 4c) achieved their highest values (30–40 ppt) during this time period, with peak values of 35–40 ppt extending into June and the start of the wet season. Such high salinities have previously been shown to contribute to reduced stomatal conductance and lowered net carbon assimilation at the leaf-level (Barr et al., 2009) during the afternoon. Surface water salinities above 28 ppt also result in reduced NEE at the ecosystem scale (Barr et al., 2010). PAR declined throughout the wet season following the summer solstice in June, coincident with reduced salinity levels resulting from increased freshwater flow through Shark River. Seasonal minima in salinity of 15–20 ppt occurred at the end of the wet season in October and November. Productivity was predicted to be seasonally lowest during December and January, when air temperatures were below 20 °C and when PAR reached seasonal minima of 20–30 mol photons m⁻² per day, coincident with the winter solstice. During the extended cold spell of January 2010, temperatures reached nearly the freezing point during several early morning periods, with an 8-day average of approximately 10 °C. Premature abscission of leaves in the canopy crown was observed on site, and likely resulted in reduced productivity and GPP.

3.4 Canopy-scale CO₂ fluxes

During the year-round growing season, this forest exhibited pronounced seasonal NEE patterns. Seasonal maxima in daily CO₂ uptake by the forest were observed during March to May in 2004–2005 (Fig. 5a). Secondary peaks were observed during the month of November both before and after the hurricane. R_E values (Fig. 5b) were seasonally highest during June to August with 8-day averages of 0.30–0.40 and 0.30–0.55 mol C m⁻² day⁻¹ during 2004–2005 and 2007–2011, respectively. R_E values were lowest between December and April. GPP (Fig. 5c) values were lowest during January and February, coincident with seasonal minima in PAR and T_A, and exhibited broad seasonal maxima between April and October, with values of 0.50–0.63 and
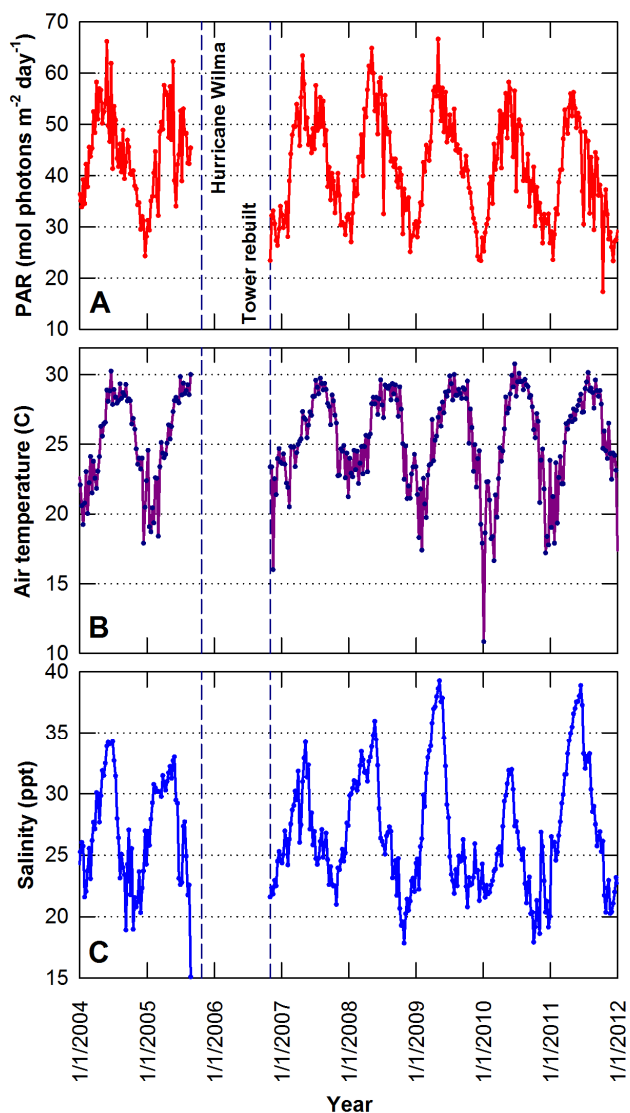
Fig. 4. Eight-day averages of photosynthetic active irradiance, PAR; $mol\,(photons)\,m^{-2}\,day^{-1}$ **(A)** and air temperature (°C) **(B)** at a height of 27 m at the SRS6 tower site. Eight-day average surface water salinities (ppt) **(C)** measured from a well at the USGS SH3 site adjacent to the tower.

Fig. 5. Eight-day sums of $-$NEE, $mol\,C\,m^{-2}\,day^{-1}$ **(A)** from the SRS6 tower site and derived products including ecosystem respiration, R_E; $mol\,C\,m^{-2}\,day^{-1}$ **(B)**, gross primary productivity, GPP; $mol\,C\,m^{-2}\,day^{-1}$ **(C)**, and light (PAR) use efficiency LUE; $mmol\,C\,(mol\,photons)^{-1}$ **(D)**.

$0.50–0.75\,mol\,C\,m^{-2}\,day^{-1}$ during 2004–2005 and 2007–2011, respectively. LUE and PAR exhibited a strong negative correlation ($R^2 = -0.70$), suggesting that this ecosystem has adapted a physiological strategy for maintaining high GPP rates throughout most of the year. Elevated GPP values during cloudy days may be caused by higher fractions of diffuse compared to direct solar irradiance penetrating to lower canopy layers and raising the whole canopy LUE (Barr et al., 2010). Other forests experience enhanced C assimilation when subject to elevated diffuse irradiance (Gu et al., 2003).
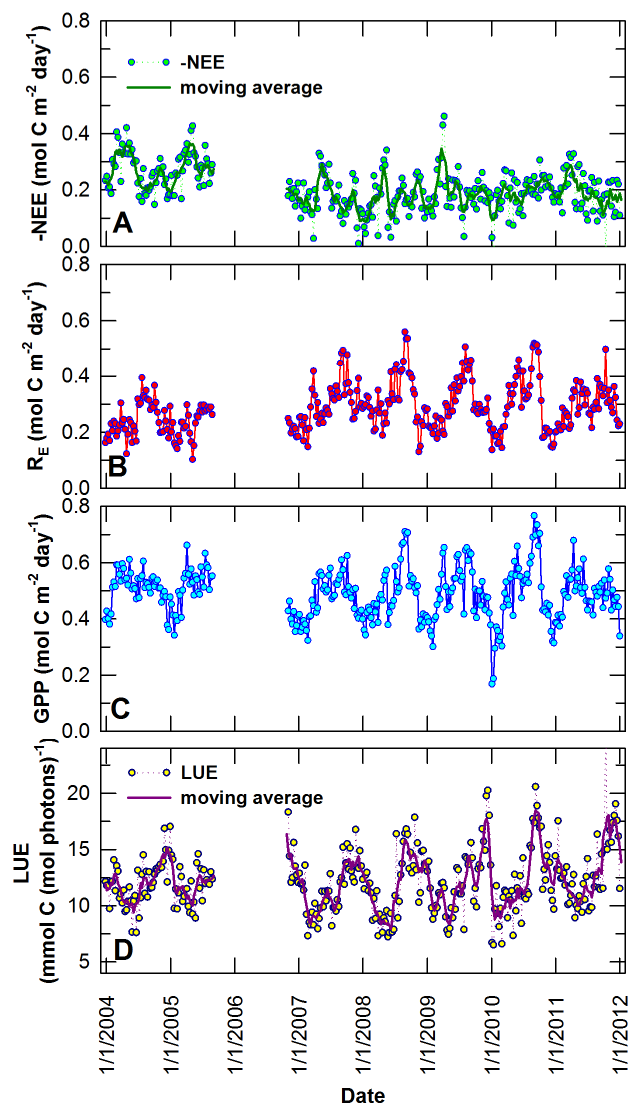
3.5 Light use efficiency

Seasonal LUE patterns (Fig. 5d) were different compared to GPP and exhibited seasonal maxima (13–20 $mmol\,C\,(mol\,PAR)^{-1}$) during the months of September to December, while PAR and salinity levels were declining or at their seasonal minima. LUE values generally declined with the progression of the dry seasons, reaching annual minima of 7–10 $mmol\,C\,(mol\,PAR)^{-1}$ during the months of April to June, with some interannual variability. For example, in January 2010, LUE declined from an 8-day average of 19 to 6 $mmol\,C\,(mol\,PAR)^{-1}$ from 19 December 2009 to 4 January 2010. This period coincided with several weeks of nighttime

temperatures that approached 0 °C. These cold air masses induced foliage senescence and extensive litterfall. Salinity represents an important control on mangrove forest LUE, and therefore on ecosystem productivity. The regression analyses that relate the 8-day average LUE (i.e., $LUE/LUE_{salinity=0}$) to salinity (Fig. 6) provided a 1.5 % reduction in this ratio for every 1 ppt salinity increase. However, the relationship between $LUE/LUE_{salinity=0}$ and salinity was heteroscedastic and suggested that salinity was one of several forcings required in the MVP-LUE model in relationship Eq. (7). The linear forcing was also consistent with previous results (Barr et al., 2010) and showed that midday LUE declined linearly with increasing salinity, resulting in a 48 % reduction in LUE from the lowest (16.7 ppt) to highest (34.7 ppt) salinity recorded during the 2004–2005 study period. The observed reductions in LUE were also consistent with previous studies (Ball and Pidsley, 1995; Sobrado, 1999; Krauss and Allen, 2003; Parida et al., 2004) that indicated declines in leaf-level C assimilation in response to increasing soil water salinity. By extrapolating the observed linear decline in LUE, the productivity of the mangrove ecosystem ceases at surface water salinity approaching 70 ppt according to the model expressed in relationship Eq. (7). Whereas such high salinity levels do not occur at the Everglades study site, this estimate is in close agreement with average salinity tolerances of 60–90 ppt reported for red, white, and black mangroves (Odum et al., 1982).

3.6 MVP-LUE model results

The cross-validated LUE model (Sect. 2.4) was capable of reproducing the observed responses of LUE and GPP to seasonal changes in environmental variables and recovery from a major hurricane disturbance. The median and 95 % uncertainty bounds of modeled mean LUE, μ_{LUE} (Fig. 7), provided posterior predictions from 10 000 MCMC iterations in each of 3 independent chains determined from 5-fold cross validation. The largest discrepancies between estimated and modeled mean LUE occurred during March to May of 2007 and 2008, when estimated LUE were seasonally lowest. Posterior means calculated over the full 2004–2011 period of record were evaluated by the Pearson's correlation coefficient (R), the coefficient of efficiency (CoE), and the normalized bias (NB). The model performed nearly as well during validation ($R^2 = 0.646$, CoE $= 0.645$; NB $= -0.015$) as during training ($R^2 = 0.651$, CoE $= 0.651$; NB $= -0.015$).

Posterior distributions of model forcings (Table 1) allowed estimates of mangrove productivity in response to key forcings, including EVI, air temperature, and salinity. The positive m_{EVI} (4.03 ± 0.52; mean ± 1 s.d.) confirmed that fPAR, and therefore LUE, increased with EVI values. Air temperatures of 27.8 ± 0.3 °C (mean ± 1 s.d.) favored optimal mangrove LUE. These temperatures (Fig. 4b) occurred most frequently during March to May and October to November. Both modeled and estimated LUE val-
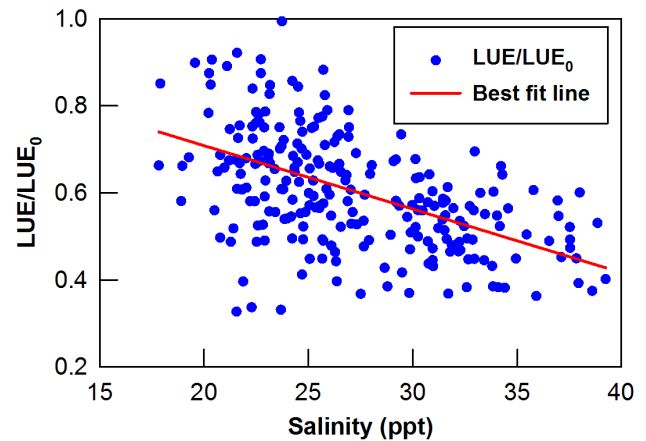

Fig. 6. Eight-day average light use efficiency (LUE) normalized by the extrapolated LUE, LUE_0 at a salinity value of 0 ppt during 2004–2005 and November 2006 to December 2011. The best fit line (slope $= -0.0146$ and intercept $= 1.0$) represents the predicted decline in fractional LUE with 8-day average salinity beginning at a value of 1.0 at zero salinity.

ues declined as air temperatures approached the T_{Max} value of 33.5 ± 0.6 °C. The slope m_{sal} (0.0047 ± 0.0022) of the salinity forcing f_{sal} was a factor of three lower compared to the slope (0.0146) determined from the response of $LUE/LUE_{salinity=0}$ to salinity (Fig. 6). This apparent sharper decline in LUE with increasing salinity masked the effect of increasing PAR on LUE since seasonal PAR peaks in nearly the same season (May–June) as salinity. The Bayesian model results suggest that LUE significantly declined with increasing PAR, with a slope m_{PAR} of 0.0101 ± 0.0004 (Table 1). Photosynthetic saturation with increasing PAR is currently not included in many light-use-efficiency-based models of productivity using satellite data (e.g., Xiao et al., 2004; Cook, et al., 2008; Chen et al., 2010). An increase from the lowest (15 ppt) to highest (39 ppt) salinity values observed during the study period was predicted to result in an 11 % reduction in LUE. Also, an increase in PAR from the lowest (17 mol photons m^{-2} day^{-1}) to highest (67 mol photons m^{-2} day^{-1}) 8-day average during 2004–2011 resulted in a 51 % reduction in LUE.

Air temperature, salinity, PAR, and EVI were all determined as significant predictors of LUE (Fig. 7). Low temperatures (~ 10 °C) during passages of cold fronts can last from a few days to weeks during December to February, resulting in large reductions in LUE and therefore GPP. For instance, the passage of cold fronts during January 2010 resulted in estimated and modeled LUE of ~ 6 mmol C (mol photons)$^{-1}$. While other controls on LUE remained constant, a change in air temperature from 28 °C (optimum temperature) to 10 °C was predicted to result in a 65 % reduction in LUE. These results confirm that mangrove forests become severely stressed when daily average temperatures drop below ~ 5 °C. Ross

Table 1. MVP-LUE model forcing terms and associated uncertainty bounds.

Parameter	Description	Mean	SD	2.50 %	Median	97.50 %
ε_0	Optimum light use efficiency ($\text{mmol C} \, (\text{mol photons})^{-1}$)	31.8	2.2	27.7	31.6	36.7
m_{EVI}	Curvature of fPAR response to EVI (dimensionless)	4.03	0.52	3.11	3.99	5.21
T_{min}	Temperature minimum (°C)	2.6	0.6	1.4	2.7	3.7
T_{max}	Temperature maximum (°C)	33.5	0.6	32.4	33.5	34.8
T_{opt}	Temperature optimum (°C)	27.8	0.3	27.2	27.8	28.5
m_{sal}	Salinity forcing (dimensionless)	0.0047	0.0022	0.0000	0.0048	0.0084
m_{PAR}	PAR saturation forcing	0.0101	0.0004	0.0092	0.0102	0.0110
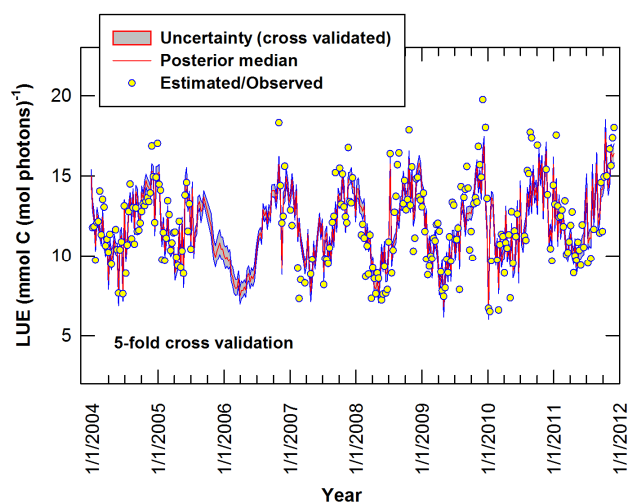
Fig. 7. Eight-day average estimated LUE and modeled mean LUE, μ_{LUE} ($\text{mmol C} \, (\text{mol photons})^{-1}$) at the tower site during 2004 through 2011. LUE estimates were not available from August 2005 through October 2006. The line (red) represents the posterior median μ_{LUE} and shaded area represents the 2.5 % and 97.5 % uncertainty bounds of μ_{LUE}. Uncertainties are provided for validation data sets derived from 5-fold cross validation. Modeled mean LUE is controlled by 8-day averages of EVI, air temperature at 27 m, and surface water salinity.

et al. (2009) measured high mangrove mortality following freeze events, and the inability of mangroves to survive in climates where temperatures near the freezing point are frequent.

3.7 MVP-LUE and MODIS GPP compared to EC GPP estimates

The calibrated MVP-LUE model provided an improved mechanistic understanding of mangrove forest productivity compared to the standard MODIS GPP product. Specifically, least-squares linear regressions of 8-day MVP-LUE modeled GPP values to EC-estimated GPP (Fig. 8a) indicated improved performance during 2004–2005 (slope = 0.720, in-

tercept = 0.144, $R^2 = 0.56$) compared to the 2006–2011 period following hurricane disturbance (slope = 0.483, intercept = 0.249, $R^2 = 0.45$). The regression of MODIS GPP to EC-estimated GPP (Fig. 8b) suggested that the uncalibrated MODIS model only weakly captured productivity trends during 2004–2005 (slope = 0.477, intercept = 0.238, $R^2 = 0.050$), and failed to capture any trends in GPP during 2006–2011 (slope = −0.372, intercept = 0.597, $R^2 = 0.056$). The MVP-LUE model captured the broad seasonal maxima ($0.5–0.7 \, \text{mol C} \, \text{m}^{-2} \, \text{day}^{-1}$) in EC-estimated GPP (Fig. 9) as a result of the strong dependence of mangrove forest productivity on air temperature. However, a mechanism to describe the short-lived (8 to 24 days) peaks in GPP of $0.6–0.75 \, \text{mol C} \, \text{m}^{-2} \, \text{day}^{-1}$ was not identified. During December to February, temperatures below ~ 20 °C, and to a lesser extent shorter day length and daily PAR, resulted in short-lived minima in GPP of $0.2–0.35 \, \text{mol C} \, \text{m}^{-2} \, \text{day}^{-1}$. The productivity response of mangrove forests to temperature has not been calibrated in the MODIS product and may partially explain the lack of correlation between MODIS GPP and EC-estimates. Also, the increased variance in MODIS GPP compared to EC-estimates (Fig. 8b) may be attributed to the MODIS model structure, which considers GPP as linearly increasing with PAR. The dampened GPP response to PAR identified in the MVP-LUE model resulted in seasonal variability in GPP better matching observations. Also, the MVP-LUE model captured the sustained plateau in EC-estimated GPP into November. This resulted from lowered salinity stress during September to November represented in the model (Eq. 7) and a modulated response of GPP to daily PAR integrals represented by the decline in LUE with increasing PAR (Eq. 8).

4 Summary and conclusions

This research represents a first attempt to design and verify a light use efficiency model for mangroves through the integration of remotely sensed information, and meteorological and hydrologic data. This study is the first one to quantify the respiratory responses of mangrove forests over temporal scales
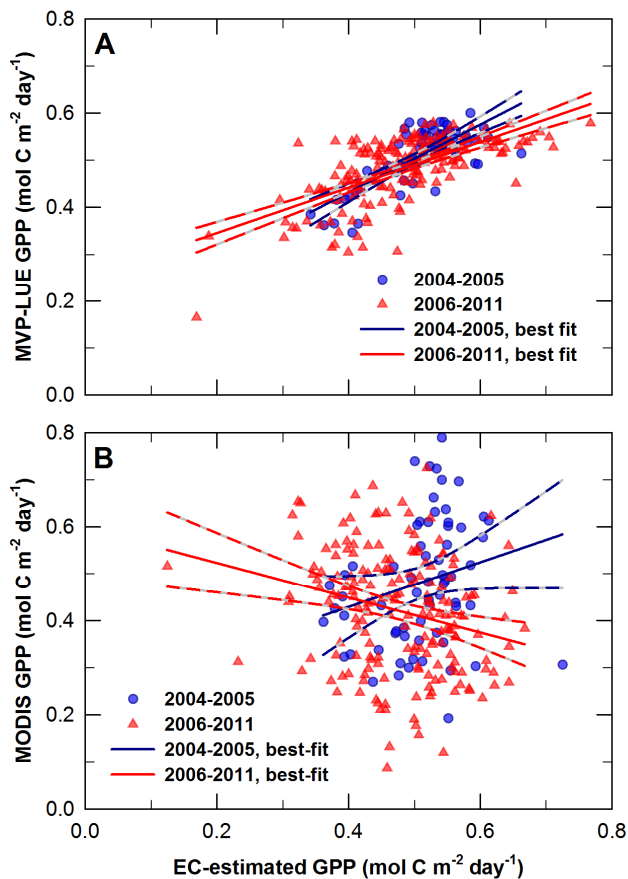
Fig. 8. Eight-day averages of MVP-LUE modeled GPP (LUE × PAR) versus 8-day averages of EC-estimated GPP during 2004–2005 and 2006–2011 (**A**). Best-fit lines were determined from least-squares linear regression and include 95 % confidence bands for the best-fit line during 2004–2005 (slope = 0.720, intercept = 0.144, $R^2 = 0.56$) and 2006–2011 (slope = 0.483, intercept = 0.249, $R^2 = 0.45$). 8-day averages of MODIS GPP versus 8-day averages of eddy covariance estimated GPP (**B**) and best-fit lines during 2004–2005 (slope = 0.477, intercept = 0.238, $R^2 = 0.050$) and 2006–2011 (slope = -0.372, intercept = 0.597, $R^2 = 0.056$).

Fig. 9. Eight-day averages of EC-estimated and MVP-LUE modeled GPP (LUE × PAR) and 3-period moving average of modeled GPP during 2004–2011.

of several growing seasons. Ecosystem respiration was successfully modeled using an atypical response function that includes a high-temperature ($\sim 33\,^\circ$C) deactivation term. Estimation of the temporally and temperature-dependent response of ecosystem respiration to air temperature provided a critical first step in modeling mangrove GPP.

Observed seasonal patterns in 8-day LUE were controlled by variability in daily PAR and air temperature, and to a lesser extent salinity and EVI fluctuations. LUE was lower when seasonal PAR was highest during April and May as a result of photosynthetic saturation. Also, salinity maxima of 35 to 40 ppt contributed to canopy-scale reductions in LUE during April to early June, amounting to a 5 % reduction in LUE per each 10 ppt increase in salinity. Lowered LUE val-
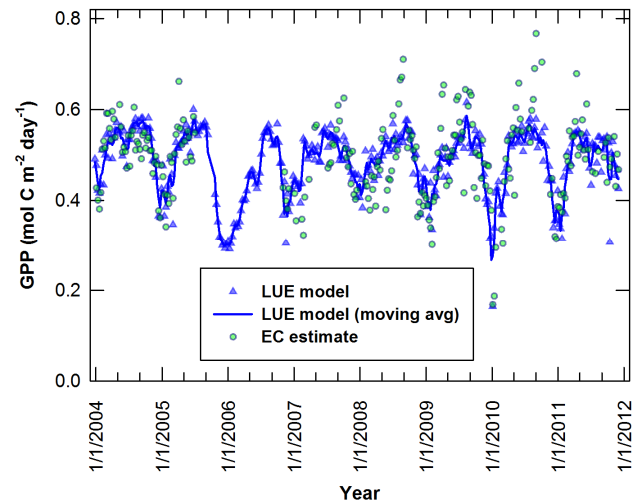
ues during December and January were the result of lower air temperatures and lowered physiological activity. As temperatures approach 3 °C, our model predicts that CO_2 uptake in these forests approaches zero. Significantly reduced EVI values after Hurricane Wilma in 2005 also resulted in significantly lowered model estimates of CO_2 uptake during the period when the EC tower was not operating. These results suggest that mangrove forest LUE can be quite variable in subtropical environments that experience seasonal variations in solar irradiance and air temperature, and disturbance from tropical storms.

The model and functional relationships determined in this study provide an important first step for understanding the larger role mangrove forests play in both regional and global C budgets. Remote sensing applications building on these results provide a means to estimate CO_2 fluxes in areas outside the flux tower footprint and in other mangrove forests around the tropics and subtropics. To do this, spatiotemporal patterns in salinity are required as model input, which may be resolved, as in the Everglades, from networks of hydrologic monitoring stations. PAR and air temperature data fields are also required. However, validating this model in locations not equipped with EC will require novel approaches that link predicted GPP values to other measurable parameters, such as biomass accumulation, or NECB at appropriate time scales. As more EC towers are deployed in other types of mangrove forests, LUE models such as this one may be used to identify patterns in quantum efficiencies across species, across forest structural characteristics (e.g., scattered or dwarf forests), and latitudinal position. The integrated datasets in turn will enable more precise approximations of the role mangrove forests play in global C dynamics.

References

Alongi, D. M., Sasekumar, A., Chong, V. C., Pfizner, J., Trott, L. A., Tirendi, F., Dixon, P., and Brunskill, G. J.: Sediment accumulation and organic material flux in a managed mangrove ecosystem: estimates of land-ocean-atmosphere exchange in peninsular Malaysia, Mar. Geol., 208, 383–402, 2004.

Ball, M. C. and Pidsley, S. M.: Growth responses to salinity in relation to distribution of two mangrove species, Sonneratia alba and S. lanceolata, in northern Australia, Funct. Ecol., 9, 77–85, 1995.

Barr, J. G., Fuentes, J. D., Wang, D., Edmonds, Y., Zieman, J. C., Hayden, B. P., and Childers, D.: Red mangroves emit hydrocarbons, Southeast. Nat., 2, 499–510, 2003.

Barr, J. G., Fuentes, J. D., Engel, V., and Zieman, J. C.: Physiological responses of red mangroves to the climate in the Florida Everglades, J. Geophys. Res., 114, G02008, doi:10.1029/2008JG000843, 2009.

Barr, J. G., Engel, V., Fuentes, J. D., Zieman, J. C., O'Halloran, T. L., Smith, T. J., and Anderson, G. H.: Controls on mangrove forest-atmosphere carbon dioxide exchanges in western Everglades National Park. J. Geophys. Res.-Biogeo., 115, 1–14, doi:10.1029/2009JG001186, 2010.

Barr, J. G., Engel, V., Smith, T. J., and Fuentes, J. D.: Hurricane disturbance and recovery of energy balance, CO_2 fluxes and canopy structure in a mangrove forest of the Florida Everglades, Agr. Forest Meteorol., 153, 54–66, doi:10.1016/j.agrformet.2011.07.022, 2012.

Campbell, G. S. and Norman, J. M.: An Introduction to Environmental Biophysics – 2nd Edn., Springer, New York, 286 pp., 1998.

Casella, G. and George, E. I.: Explaining the Gibbs sampler, Am. Stat., 46, 167–174, 1992.

Castaneda, E.: Landscape patterns of community structure, biomass, and net primary productivity of mangrove forests in the Florida Coastal Everglades as a function of resources, regulators, hydroperiod, and hurricane disturbance, Ph.D. Dissertation, Louisiana State University, Lafayette, 171 pp., 2010.

Chapin, F. S., Woodwell, G. M., Randerson, J. T., Rastetter, E. B., Lovett, G. M., Baldocchi, D. D., Clark, D. A., Harmon, M. E., Schimel, D. S., Valentini, R., Wirth, C., Aber, J. D., Cole, J. J., Goulden, M. L., Harden, J. W., Heimann, M., Howarth, R. W., Matson, P. A., McGuire, A. D., Melillo, J. M., Mooney, H. A., Neff, J. C., Houghton, R. A., Pace, M. L., Ryan, M. G., Running, S. W., Sala, O. E., Schlesinger, W. H., and Schulze, E.-D.: Recon-

ciling carbon-cycle concepts, terminology, and methods, Ecosystems, 9, 1041–1050, doi:10.1007/s10021-005-0105-7, 2006.

Chen, B., Ge, Q., Fu, D., Yu, G., Sun, X., Wang, S., and Wang, H.: A data-model fusion approach for upscaling gross ecosystem productivity to the landscape scale based on remote sensing and flux footprint modelling, Biogeosciences, 7, 2943–2958, doi:10.5194/bg-7-2943-2010, 2010.

Cook, B. D., Bolstad, P. V., Martin, J. G., Heinsch, F. A. Davis, K. J., Wang, W., Desai, A. R., and Teclaw, R. M.: Using light-sue and production efficiency models to predict photosynthetic and net carbon exchange during forest canopy disturbance, Ecosystems, 11, 26–44, doi:10.1007/s10021-007-9105-0, 2008.

Donato, D. C., Kauffman, J. B., Murdiyarso, D., Kurnianto, S., Stidham, M., and Kanninen, M.: Mangroves among the most carbon-rich forests in the tropics, Nat. Geosci., 4, 293–297, doi:10.1038/ngeo1123, 2011.

Gelman, A., Carlin, J. B., Stern, H. S., and Rubin, D. B.: Bayesian Data Analysis, 2nd Edn., Chapman and Hall/CRC, Boca Raton, FL, 696 pp., 2004.

Gilks, W. R., Best, N. G., and Tan, K. K. C.: Adaptive rejection metropolis sampling within Gibbs sampling, Appl. Stat. J. Roy. St. Soc. C, 44, 455–472, 1995.

Goetz, S. J., Prince, S. D., Goward, S. N., Thawley, M. M., and Small, J.: Satellite remote sensing of primary production: an improved production efficiency modeling approach, Ecol. Model., 122, 239–255, 1999.

Gu, L., Baldocchi, D. D., Wofsy, S. E., Munger, J. W., Michalsky, J. J., and Boden, T. A.: Response of a deciduous forest to the Mt. Pinatubo eruption: enhanced photosynthesis, Science, 299, 2035–2038, 2003.

Heinsch F. A., Zhao, M., Running, S. W., Kimball, J. S., Nemani, R. R., Davis, K. J., Bolstad, P. V., Cook B. D., Desai, A. R., Ricciuto, D. M., Law, B. E., Oechel, W. C., Kwon, H., Luo, H., Wofsy, S. C., Dunn, A. L., Munger, J. W., Baldocchi, D. D., Xu, L., Hollinger, D. Y., Richardson, A. D., Stoy, P. C., Siqueira, M. B. S., Monson, R. K., Burns, S. P., and Flanagan, L. B.: Evaluation of remote sensing based terrestrial productivity from MODIS using regional tower eddy flux network observations, IEEE T. Geosci. Remote, 44, 1908–1925, 2006.

Huete, A., Didan, K., Miura, T., Rodriguez, E. P., Gao, X., and Ferreira, L. G.: Overview of the radiometric and biophysical performance of the MODIS vegetation indices, Remote Sens. Environ., 83, 195–213, 2002.

Jiang, Z., Huete, A. R., Didan, K., and Miura, T.: Development of a two-band enhanced vegetation index without a blue band, Rem. Sens. Environ., 112, 3833–3845, 2008.

Krauss, K. W. and Allen, J. A.: Influences of salinity and shade on seedling photosynthesis and growth of two mangrove species, Rhizophora mangle and Bruguiera sexangula, introduced to Hawaii, Aquat. Bot., 77, 311–324, 2003.

Laffoley, D. and Grimsditch, G.: The Management of Natural Coastal Carbon Sinks, IUCN, Gland, 2009.

Lloyd, J. and Taylor, J. A.: On the temperature dependence of soil respiration, Funct. Ecol., 8, 315–323, doi:10.2307/2389824, 1994.

Lovelock, C. E.: Soil respiration and belowground carbon allocation in mangrove forests, Ecosystems, 11, 342–354, doi:10.1007/s10021-008-9125-4, 2008.

Mayorga, E., Aufdenkampe, A. K., Masiello, C. A., Krusche, A. V., Hedges, J. I., Quay, P. D., Richey, J. E., and Brown, T. A.: Young organic matter as a source of carbon dioxide outgassing from Amazonian rivers, Nat. Lett., 436, 538–541, doi:10.1038/nature03880, 2005.

Monteith, J. L.: The photosynthesis and transpiration of crops, Exp. Agr., 2, 1–14, 1966.

Monteith, J. L.: Solar radiation and productivity in tropical ecosystems, J. Appl. Ecol., 9, 747–766, 1972.

Odum, W. E., Mclvor, C. C., and Smith III, T. J.: The ecology of the mangroves of south Florida: a community profile, U.S. Fish and Wildlife Service, Office of Biological Services, Washington DC, FWS/OBS-81/24, 144 pp., Reprinted September 1985, 1982.

O'Hagan, A. and Forster, J. J.: Kendall's Advanced Theory of Statistics: Bayesian Inference. 2B (2nd Edn.), Arnold, New York, NY, ISBN 0-340-80752-0, 2004.

Parida, A. K., Das, A. B., and Mittra, B.: Effects of salt on growth, ion accumulation, photosynthesis and leaf anatomy of the mangrove, Bruguierra parviflora, Trees, 18, 167–174, 2004.

Potter, C.: The carbon budget of California, Environ. Sci. Policy, 13, 373–383, 2010.

Prince, S. D. and Goward, S. N.: Global primary production: A remote sensing approach, J. Biogeogr., 22, 815–835, 1995.

Raich, J. W., Rastetter, E. B., Melillo, J. M., Kicklighter, D. W., Steudler, P. A., Peterson, B. J., Grace, A. L., Moore, B., and Vorosmarty, C. J.: Potential net primary productivity in South America: application of a global-model, Ecol. Appl., 1, 399–429, 1991.

Reichstein, M., Falge, E., Baldocchi, D., Papale, D., Aubinet, M., Berbigier, P., Bernhofer, C., Buchmann, N., Ilmanov, T.G. Granier, A., Grunwald, T., Havrankova, K., Ilvesniemi, H., Janous, D., Knohl, A., Laurila, T., Lohila, A., Loustau, D., Matteucci, G., Meyers, T., Miglietta, F., Ourcival, J.-M., Pumpanen, J., Rambal, S., Rotenberg, E., Sanz, M., Tenhunen, J., Seufert, G., Vaccar, F., Vesala, T., Yaki, D., and Valentini, R.: On the separation of net ecosystem exchange into assimilation and ecosystem respiration: review and improved algorithm, Glob. Change Biol., 11, 1424–1439, doi:10.1111/j.1365-2486.2005.001002.x, 2005.

Romigh, M. M., Davis III, S. E, Rivera-Monroy, V. H., and Twilley, R. R.: Flux of organic carbon in a riverine mangrove wetland in the Florida Coastal Everglades, Hydrobiologia, 569, 505–516, 2006.

Ross, M. S., Ruiz, P. L., Sah, J. P., and Hanan, E. J.: Chilling damage in a changing climate in coastal landscapes of the subtropical zone: a case study from south Florida, Glob. Change Biol., 15, 1817–1832, doi:10.1111/j.1365-2486.2009.01900.x, 2009.

Running, S. W., Baldocchi, D. D., Turner, D. P., Gower, S. T., Bakwin, P. S., and Hibbard, K. A.: A global terrestrial monitoring network integrating tower fluxes, flask sampling, ecosystem modeling and EOS satellite data, Rem. Sens. Environ., 70, 108–128, 1999.

Running, S. W., Thornton, P. E., Nemani, R. R., and Glassy, J. M.: Global terrestrial gross and net primary productivity from the earth observing system, in: Methods in ecosystem science, edited by: Sala, O., Jackson, R., and Mooney, H., Springer, New York, 44–57, 2000.

Schubert, P., Lund, M., Ström, L., and Eklundh, L.: Impact of nutrients on peatland GPP estimations using MODIS time series data, Rem. Sens. Environ., 114, 2137–2145, 2010.

Shank, G. C., Zepp, R. G., Vahatalo, A., Lee, R., and Bartels, E.: Photobleaching kinetics of chromophoric dissolved organic matter derived from mangrove leaf litter and floating Sargassum colonies, Mar. Chem., 119, 162–171, doi:10.1016/j.marchem.2010.01.003, 2010.

Sobrado, M. A.: Leaf photosynthesis of the mangrove Avicennia germinans as affected by NaCl, Photosynthetica, 36, 547–555, 1999.

Souza, M. F. L., Gomes, V. R., Freitas, S. S., Andrade, R. C. B., and Knoppers, B.: Net ecosystem metabolism and nonconservative fluxes of organic matter in a tropical mangrove estuary, Piauí River (NE of Brazil), Estuar. Coast., 32, 111–122, doi:10.1007/s12237-008-9104-1, 2009.

Spiegelhalter, D., Thomas, A., Best N., and Lunn, D.: WinBUGS User Manual, Version 1.4, MRC Biostatistics Unit, Cambridge, UK, 2003.

Strangmann, A., Bashan, Y., and Giani, L.: Methane in pristine and impaired mangrove soils and its possible effect on establishment of mangrove seedlings Biol. Fertil. Soils, 44, 511–519, doi:10.1007/s00374-007-0233-7, 2008.

Tucker, C. J., Vanpraet, C., Boerwinkel, E., and Gaston, A.: Satellite remote sensing of total dry matter production in the Senegalese Sahel, Rem. Sens. Environ., 13, 461–474, 1983.

Turner, D. P., Ritts, W. D., Cohen, W. B., Gower, S. T., Running, S. W., Zhao, M., Costa, M. H., Kirschbaum A., Ham, J., Saleska, S., and Ahl, D.: Evaluation of MODIS NPP and GPP products across multiple biomes, Rem. Sens. Environ., 102, 282–292, 2006.

Vargas, R. and Allen, M. F.: Diel patterns of soil respiration in a tropical forest after Hurricane Wilma, J. Geophys. Res., 113, G03021, doi:10.1029/2007JG000620, 2008.

Xiao, X., Hollinger, D., Aber, J. D., Goltz, M., Davidson, E., Zhang, Q., and Moore III, B.: Satellite-based modeling of gross primary production in an evergreen needle leaf forest, Rem. Sens. Environ., 89, 519–534, 2004.

Zhao, M. and Running, S. W.: Remote sensing of terrestrial Primary Production and Carbon Cycle, in: Advances in Land Remote Sensing: System, Modeling, Inversion and Application, edited by: Liang, S., Springer Science, 423–444, 2008.

Zhao, M., Heinsch, F. A., Nemani, R. R., and Running, S. W.: Improvements of the MODIS terrestrial gross and net primary production global dataset, Rem. Sens. Environ., 95, 164–176, 2005.